Scaling behavior of universal pinch-off in two-dimensional foam

Chin-Chang Kuo and Michael Dennin

Phys. Rev. E **87**, 052308 — Published 22 May 2013

DOI: 10.1103/PhysRevE.87.052308

Scaling behavior of universal pinch-off in two-dimensional foam

Chin-Chang Kuo, and Michael Dennin*
Department of Physics and Astronomy and Institute for Complex Adaptive Matter, University of California at Irvine, Irvine, CA 92697-4575

We study the power-law scaling behavior and pinch-off morphology of two-dimensional bubble rafts under tension. As a function of pulling speed, we observe two distinct pinch-off morphologies that have been observed in other fluid systems: long threads (LT) and double-cone (DC). At any given pulling speed, there is a non-zero probability of observing LT or DC, with the probability of observing LT modes increasing with pulling velocity. The bubble rafts are composed of millimeter scale bubbles, and we are able to directly observe pinch-off to the point of final separation and measure the scaling of the minimum width in time. For both the LT and DC modes, the final scaling regime before pinch-off exhibits a universal power-law scaling behavior, with power-law fitting exponents of 0.73 ± 0.01. However, the final cone-angle is different for states that initially exhibit LT or DC pinch-off, and for the LT case, the final scaling is best described as a local double-cone mode.

PACS numbers: 83.60.Wc,83.80.Iz,83.50.Jf

I. INTRODUCTION

The failure modes of fluids under tension have been the subject of significant study and are relevant to a wide range of applications such as sprays, droplet formation, and thin fluid jets. The basic question is how the fluid thins as a function of time, and the ultimate separation into distinct elements. Of particular interest is the scaling behavior of various failure modes in fluids, the details of which depend on issues including the relative role of viscosity[1–7], surface tension[8–10], and even the system geometry[11–14]. Two characterizations of the failure are the shape near the pinch-off point and the scaling of the minimum radius r_{min} as a function of the time before pinch-off, given by: $r_{min} \propto (t - t_0)^n$, where t_0 is the time pinch-off occurs and n is the scaling exponent. Significant progress has been made in understanding these issues for Newtonian fluids. For 3D Newtonian fluids, the power-law exponent is $n \approx 2/3$ [3] for inviscid fluids, and $n \approx 1$ for fluids with a relatively large viscosity [9]. For 2D inviscid fluids, simulations and analytic studies indicate that the pinch-off exhibits self-similarity of the second kind [12]. One feature of this behavior is the observation of two scaling exponents: one for motion normal to the elongating direction and one for motion parallel to the elongating direction. Further, the morphology of the pinch-off of fluids generally falls into one of two categories: double-cone (DC) or long-thread (LT), where understanding the cross-over between these two morphologies is important. For example, simulations of the pinch-off of liquid propane nanobridges exhibit a cross-over between these two modes as a function of external pressure in which the probability of observing a LT mode increases with increasing pressure [15].

More recently, studies have focused on the failure modes of *complex fluids*. In these systems, the viscosity is generally dependent on the rate of strain. This significantly complicates any scaling arguments, and presents the possibility of unique and interesting failure modes. A number of complex fluids have been studied, including granular streams [16], suspensions [17–19], foams, and emulsions [20, 21]. Many of these systems exhibit a power-law dependence of the shear stress, σ, on the rate of strain: $\dot{\gamma}$ ($\sigma - \sigma_0 \propto \dot{\gamma}^m$). It has been suggested that the minimum radius during pinch-off should scale in time with the same exponent m as the shear stress dependence on rate of strain, and recent experiments have confirmed these results for 3D systems [21]. In addition, complex fluids exhibit the same basic morphologies as Newtonian fluids [16, 17, 21].

Given the generally universal behavior of pinch-off in Newtonian and complex fluids, it is natural to ask how a 2D complex fluid, such as a foam, would behave. Bubble rafts, single layers of bubbles on the water surface, are ideal 2D foam systems for studying pinch-off under tension. Previous work has established that bubble rafts under tension exhibit a pinch-off to fracture transition as a function of system size and pulling velocity, and the general dependence of this behavior on the system size and pulling speed have been studied in some detail [22, 23]. But there has not been a quantitative study of the scaling during pinch-off. In this paper, we report on both the morphology and the the scaling of pinch-off in bubble rafts under tension as a function of pulling speed. We observe a crossover of the pinch-off morphology, but the final stages of the failure exhibits

* Corresponding Authoremail: mdennin@uci.edu

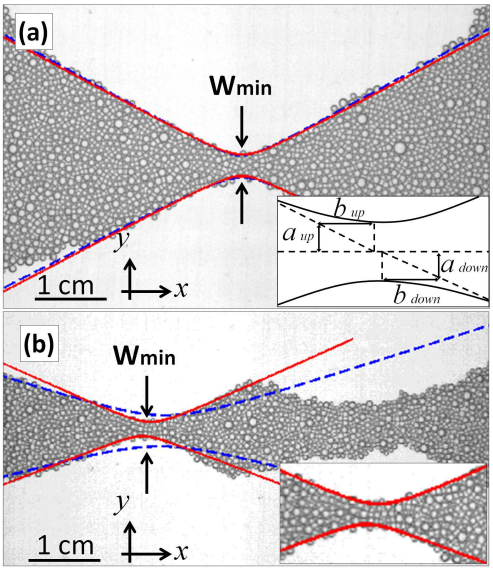

FIG. 1. Images of two main failure modes observed in the system: (a) The double-cone (DC) mode with pulling velocity of 0.86 mm/s. (b) The long-thread (LT) morphology with pulling velocity of 4.3 mm/s. The inset in (b) shows the local pinch-off morphology of the LT mode. The solid curves in the images correspond to fits of hyperbolas to the system's boundaries, either on a global (blue dash line) or a local scale (red line). The definition of the fitting parameters is shown in the insert in (a). The pinch-off of DC mode is consistent with the hyperbolic fitting for both the global and the local scale. In contrast, the pinch-off of LT mode is only consistent with the local hyperbolic fitting.

a universal power-law scaling behavior for both the normal and parallel directions relative to the pulling. The rest of the paper is organized as follows. Section II describes the experimental setup and methods of analysis. Section III provides the experimental results and a brief discussion of the scaling. Section IV is a summary of the results.

II. EXPERIMENTAL DETAILS

We used amorphous bubble rafts to study the pinch-off dynamics of a 2D complex fluid. Bubbles are created on the surface of an aqueous solution by blowing nitrogen through a solution of 5% Miracle Bubble, 15% glycerol, and 80% deionized water. The range of bubble radii is from 0.3 mm to 0.5 mm. The bubbles are formed between two polycarbonate plates. The bubbles are attracted to the polycarbonate boundary plates, and attach without any additional modifications. The separation between the plates sets the initial length of the raft, and the width of the plates sets the initial width of the raft. The sides of the raft that are perpendicular to the plates are free, and initially form relative straight boundaries. However, there are some variations in the local width along the length of the sample. The initial bubble raft width and length are 80 mm and 60 mm. The bubble rafts are elongated along the direction of raft length by moving the plates apart at constant speeds ranging from 0.0086 to 4.3 mm/s. We didn't observe any slip and detachment between bubble raft and boundaries in the experiment. Bubble raft pinch-off images are recorded by a CCD camera and processed by MATLAB for the quantitative analysis. The boundary of the bubble rafts is detected by an image threshold method and is defined as a fit to the outer edge of the bubbles. We analyzed the shape of the bubble raft under tension to study the pinch-off morphology of bubble raft. Full experimental details are described in Ref. [22, 23].

Figure 1 illustrates the two failure modes. Fig. 1(a) illustrates the double-cone (DC) failure mode for a pulling velocity of 0.86 mm/s. This failure mode is a highly symmetric configuration. Fig. 1(b) illustrates the long-thread (LT) failure mode for a pulling velocity of 4.29 mm/s. The images are at a time of 800 ms for Fig. 1(a)and 240 ms for Fig. 2(b) before the pinch-off. The evolution of the LT systems has two distinct stages. Initially, the system has essentially a uniform width along its length that thins as a function of time. Eventually, variations in the width grow, and a local region develops a DC morphology that produces the final pinch-off. The image Fig. 1(b) is taken at the initial formation of a local DC region, which is highlighted in the insert in Fig. 1(b). (For videos of the pinch-off process, refer to the supplementary information [24].)

We characterize the pinch-off by the minimum bubble raft width (W_{min}), i.e. the narrowest point of the bubble raft as indicated in Fig.1. Additionally, we fit the global shape of the bubble raft to a pair of hyperbolas (blue dash line in Fig.1) using $(y-y_0)^2/a^2-(x-x_0)^2/b^2 = 1$ and the coordinate system in Fig.1. Fitting the top and bottom boundaries separately gives two sets of parameters: (a_{up}, b_{up}) and (a_{down}, b_{down}). The parameter $a' = a_{up} + a_{down}$ is identical to W_{min} when the global fit is accurate. The scaling normal to the pulling direction is provided by W_{min} and a'. For scaling parallel to the pulling direction, we use $b' = (b_{up} + b_{down})$. We also use a local fit to the hyperbola, where the length of the fitting region is proportional to W_{min} (red line in Fig.1). The local fit is most relevant to the late-time behavior of the LT mode for which the global fitting procedure fails, as shown in Fig.1(b).

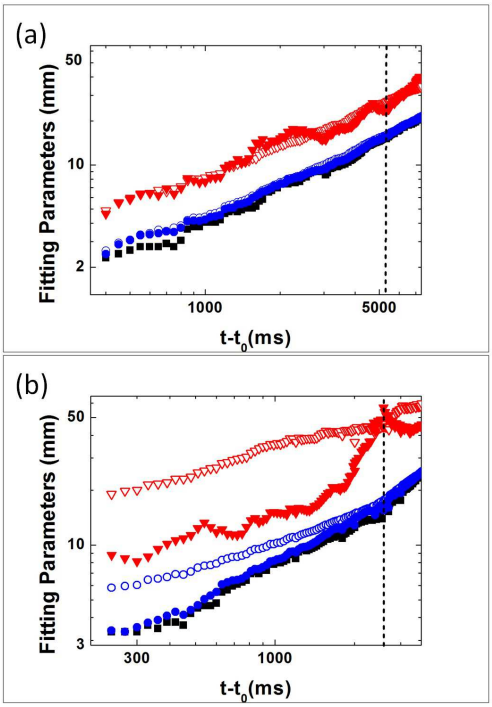

FIG. 2. The power-law scaling behaviors of typical DC (a) and LT (b) modes are shown in Fig.1. We plot the minimum bubble raft width (W_{min})(solid black square), hyperbolic fitting parameters of a' and b' in the global scale (open blue circle and open red down triangle), and in the local scale (solid blue circle and solid red down triangle) as a function of $t - t_0$ in log-log scale. Dash lines in plots indicate the time after which we consistently observe power-law scaling for W_{min}.

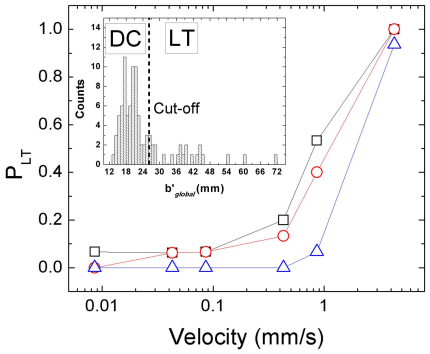

FIG. 3. The histogram of b'_{global} for three particular pulling velocities are shown in (a). Pulling velocities are 0.0086 mm/s (black), 0.86 mm/s (grey) , and 4.29 mm/s (empty bar). The distribution of b'_{global} shifts to higher values with the increase of the pulling velocity. The histogram of b'_{global} for the collection of pulling speeds ranging from 0.0086 to 4.3 mm/s is shown in (b). The histogram of b'_{global} for the combined pulling velocities is used to distinguish DC and LT modes. The histogram is based on the value of b'_{global} at the time corresponding to the transition to scaling behavior for W_{min}. The larger values of b'_{global} correspond to a LT morphology due to the flatness of the boundary. This division into DC and LT with a particular cutoff value for b'_{global} is indicated by the vertical dashed line.

III. RESULTS

Figure 2 illustrates the time dependence of W_{min}, a', and b' for a typical DC mode (Fig. 2a) and LT mode (Fig. 2b). The values for a' and b' are shown for both a global and local fit. The key feature of the DC mode is the agreement for a' and b' between the global and local fits, as well as the agreement between W_{min} and a'. In contrast, the LT mode shows a significant disagreement for a' and b' between the global and local fits. The reason for this is the failure of a global fit to a hyperbola to capture the relatively flat shape of the LT. However, because the ultimate failure mode of the LT is a local DC, a'_{local} is found to be consistent with W_{min}. It should be noted that in both cases, the early stage of the dynamics does not exhibit consistent power-law behavior in time. Therefore, for all fits to the data, we focus on the region to the left of the dashed line.

The morphology for any given realization of the experiment is determined from the behavior of b'_{global}. For the LT morphology, the global shape is consistent with a very "flat" hyperbola, and the "flatter" the hyperbola, the larger the value of b'_{global}. Therefore, we consider the value of b'_{global} at the beginning of the scaling regime for W_{min} (dashed line in Fig. 2), and if it exceeds a critical value, we classify the system as LT. To illustrate the process, we present to sets of data for b'_{global}. In Fig.3(a), we present the distribution of values for b'_{global} for three pulling speeds of 0.0086 mm/s, 0.86 mm/s, and 4.29 mm/s. The distribution of values for b'_{global} shifts with the increase of the pulling velocity, consistent with the increased probability of the LT mode occurring. In Fig.3(b), we present the aggregated data and show the distribution of b'_{global} values for all the pulling velocities and experimental runs. We choose a critical cut-off value of b'_{global} based on this distribution.

Figure 4 illustrates the probability of the system exhibiting the LT mode as a function of pulling velocity. As a test of the robustness of our cut-off choice, we show the probability distribution for LT modes using three cut-off values: 23 mm, 25 mm, and 30 mm. All three corresponding probability curves exhibit sufficiently similar behavior to justify our procedure. Additionally, we sample random runs to visually confirm that we are correctly distinguishing

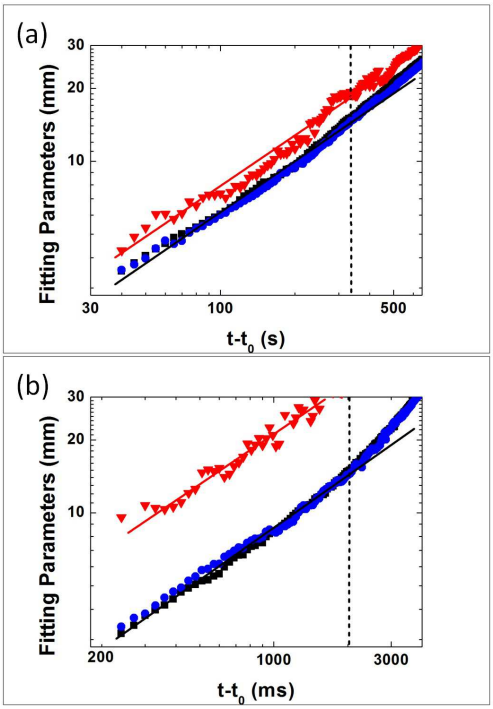

FIG. 4. The probability of observing the long-thread (LT) failure mode as a function of pulling velocity as determined by using b'_{global} and selecting three different cut-off values for the definition of LT: 23 mm (square), 25 mm (circle), and 30 mm (triangle). The plot illustrates that the qualitative behavior of the probability of observing a LT morphology is reasonably independent of the precise cut-off value, with a transition from DC dominated to LT dominated behavior around a pulling velocity of 1 mm/s.

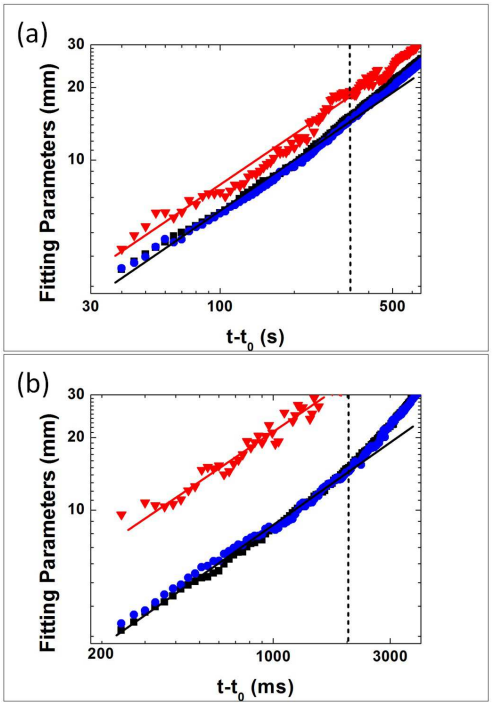

FIG. 5. Plots of the average W_{min} (black square), a'_{local} (blue circle), and b'_{local} (red down triangle) as a function of the time before pinch-off. Two pulling velocities of 0.0086 mm/s and 4.29 mm/s are shown in (a) and (b). All parameters fit to power-law scaling exponents which are all consistent with 0.73 $\pm$ 0.01. Different ratios of a'_{local} to b'_{local} in (a) and (b) are the result of variations in the pinch-off angle with pulling velocity.

LT and DC morphologies. This DC to LT transition with the increase of pulling velocity is similar to the liquid pinch-off of inviscid and viscous fluid [9]. The observed transition is at 1 mm/s and a width $\sim$ 10 mm, for a rate of strain of 0.1 s^{-1}. Interestingly, this is of the same order as the transition in confined shear flow between a quasi-static flow limit and viscous flow [25].

When the bubble raft close to the final pinch-off state, it worth noting that the global fit fails to catch the morphology of the general pinch-off shape for LT mode as shown in Fig. 1(b). To characterize the final pinch-off state for both the DC and LT modes, we focus on hyperbola fits on a local scale. In this case, the pinch-off of DC and LT mode are consistent with the local hyperbolic fitting(Fig. 1(a) and the insert of Fig. 1(b)). We average the W_{min}, a'_{local}, and b'_{local} from fifteen data sets with the same pulling velocity. The results are shown in Fig. 5 for pulling velocity of 0.0086 mm/s (a) and 4.29 mm/s (b). The plot of W_{min} , a'_{local}, and b'_{local} are as a function of $t - t_0$ for both pulling velocities. The result of the fitting exponents averaged over all runs is shown in Fig.6. There is no measurable velocity dependence of the exponents of a'_{local} and b'_{local}, and the fitting exponents are consistent with the average value of 0.73 with the standard error of 0.01 (and a standard deviation of 0.04).

At this point, we can not definitively comment on the physical meaning of the observed scaling behavior. However, there are some important features. The first question one might ask is whether or not this system is exhibiting simple scaling or self-similarity of the second kind, as found in other 2D systems. It is intriguing that theoretical work on 2D scaling found self-similarity of second kind with scaling exponents of 0.75 and 0.69 for the directions normal and parallel to the elongation, respectively [12]. However, at this point, our results strongly suggests the behavior in the bubble raft is simple scaling, with a single exponent of 0.75.

In trying to understand the source of the scaling, it is worth looking at the behavior of the pre-factors for the scaling normal ($a'_{local} = C_a(t - t_0)^n$) and paral-

lel ($b'_{local} = C_b(t - t_0)^n$) to the elongation direction. For scaling normal to the elongation direction, we find that the scaling pre-factor (C_a) is independent of the pulling velocity, except at the very highest pulling speed that is dominated by the LT morphology (see Fig. 7). For scaling parallel to the elongation direction, we find that the scaling pre-factor (C_b) exhibits a weak, logarithmic dependence on velocity. This is indicated by the fit to a straight line using a logarithmic scale for the velocity (see Fig. 8). The implications of these results will be discussed in Sec. IV.

Two additional characterizations of the failure modes are the pinch-off strain and cone angle as a function of pulling velocity, which are shown in Fig. 9. The cone angle is a local property of the morphology, and it is determined from the ratio of b'_{local} to a'_{local} from $\theta = 2\tan^{-1}(a'/b')$. The average strain at pinch-off is defined as $\Delta L/L$, where L is the initial length of the system and ΔL is the difference between the initial length and the length at pinch-off. Though this macroscopic definition of pinch-off strain may not be the physically relevant strain for determining failure, it is a useful method for providing a dimensionless time-scale for failure that can be used to compare the results for different pulling speeds. In effect, it provides an additional measure of the the likelihood of LT mood (which tends to fail at a large value of strain) and DC (which tends to fail at a smaller value of strain). As expected from the change in morphology from DC to LT in global scale, the pinch-off strain increases with pulling velocity. By definition, the LT mode stretches further than the DC mode before pinch-off. In contrast to the value of n, both the average cone angle (θ defined above) and the pinch-off strain depend on the pulling velocity. The cone angle decreases with pulling velocity, consistent with the transition from a global DC mode to a local DC failure as part of a LT mode.

IV. SUMMARY

In summary, we find two universal pinch-off morphologies when subjecting a 2D foam under tension: double cone and long thread. The occurrence of either is probabilistic, but there is a clear cross-over from DC dominated behavior to LT dominated behavior at a rate of strain similar to the cross-over to viscous dominated flow in confined shear flows. This appears consistent with the dominance of LT in highly viscosity fluids [9]. The general association of the quasi-static limit in foams with solid-like behavior suggests a comparison of the DC morphology with equivalent pinch-off behaviors in solids (see e.g. [26]). Finally, independent of the initial morphology, the ultimate failure is a local double-cone that exhibits a scaling regime with an exponent $n = 0.73 \pm 0.01$, independent of the direction relative to the pulling direction. In contrast to 3D measurements [21], this does not agree with the rheological scaling exponent of $1/3$ observed in previous bubble raft experiments [25]. However, it is similar in magnitude to simulations of a 2D inviscid fluid, though the simulations report two distinct scaling-exponents that are indicative of self-similarity of the second kind [12, 24], and only a single exponent is observed for the bubble rafts. Given these issues, even

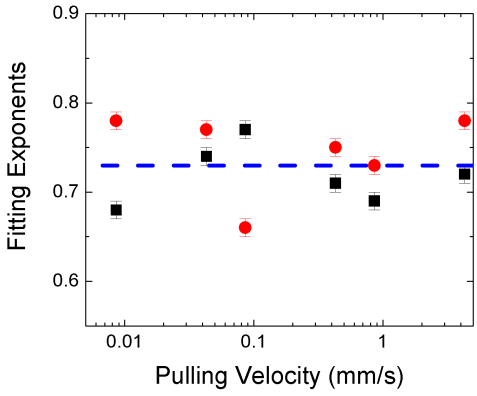

FIG. 6. The power-law fitting exponents for the average a'_{local}(black square) and b'_{local}(red circle) as a function of pulling velocity. We average fifteen runs of the a'_{local} and b'_{local} at the same pulling velocity. The results are consistent with a average value of 0.73 with a standard error of 0.01 for averaged a'_{local} and b'_{local}. We don't observe velocity dependence for the power-law fitting exponents.

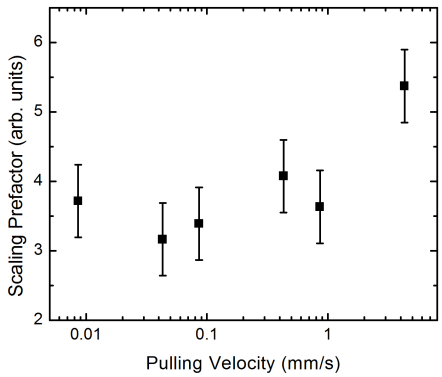

FIG. 7. The pre-factor C_a in the power-law fit of $a'_{local} = C_a(t - t_0)^n$ as a function of the pulling speed averaged over all runs. The pre-factor is found to be independent of the pulling velocity, except at the highest speeds for which the LT mode dominates.

with our limited data, it is instructive to construct a potential scaling law based on what is known.

In constructing a possible scaling law, there are two key features of the dynamics of the system that provide guidance regarding the relevant physical parameters. First, once the boundaries used to elongate the system are stopped, the pinch-off dynamics also stop. This appears to be true independent of how far the system has progressed into the pinch-off regime. Therefore, unlike the standard fluid pinch-off, this suggests that the surface tension is not a relevant parameter. Second, we find that the pre-factors in the scaling law are velocity independent (normal to the pulling direction) or only weakly dependent on the velocity (parallel to the pulling direction). Therefore, we can ignore the pulling velocity as a potential parameter. Having eliminated surface tension and driving velocity, there are only a limited number of physical parameters that can be used form a length that scales as $t^{3/4}$. First, we can consider the effective two-dimensional density of the bubble raft ρ, which has dimensions of M/L^2, where M is a mass and L is a length. For the other parameters, we have two essentially equivalent choices. From a bubble-scale perspective (which is relevant if we consider particle-based modeling of system), it is natural to consider parameters from the bubble model [27]. The bubble model essentially considers the bubble raft to be composed of circular disks with spring and viscous drag forces between them, and it has been very successful at capturing the dynamics of bubble rafts [28–32]. The two relevant parameters are: (1) an effective spring constant κ, with dimensions of force/length; and (2) a viscous dissipation term α, with dimensions of force times time/length. Constructing a length (L) that scales as time (T) to the 3/4 from these parameters gives:

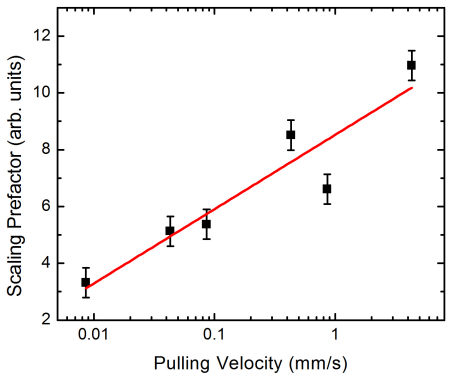

FIG. 8. The pre-factor C_b in the power-law fit of $b'_{local} = C_b(t - t_0)^n$ as a function of the pulling speed averaged over all runs. Note that a logarithmic scale is used for the x-axis to highlight the weak dependence on velocity. The line represents a linear fit to the data with the logarithmic x-axis, suggesting a logarithmic dependence on velocity.

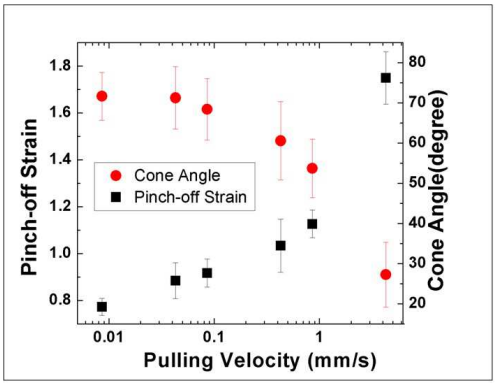

FIG. 9. The cone angle (red circle) and the pinch-off strain (black Square) versus pulling velocity: The pinch-off cone angle decreases with the pulling velocity. The pinch-off strain increases with the pulling velocity. These geometric features are expected for a transition from the DC mode to the LT mode.

$$L = \frac{(\alpha\kappa)^{1/4}}{\rho^{1/2}} T^{3/4}. \quad (1)$$

Equivalently, one could consider the macroscopic parameters that are relevant to rheological measurements of the bubble raft. One likely candidate is the yield-stress because of the fact that the dynamics are in a relatively slow velocity regime. In fact, the velocities are consistent with the quasi-static limit, where the yield-stress is known to dominate the rheological properties [25]. The other natural candidate is the bulk 2D viscosity. So, an alternative scaling law would involved the yield stress (σ_y) and the bulk 2D viscosity of the system (η), which have the same dimensions as the microscopic spring constant and the viscous dissipation terms, respectively. This would suggest a scaling law:

$$L = \frac{(\sigma_y\eta)^{1/4}}{\rho^{1/2}} T^{3/4}. \quad (2)$$

Additional work that focuses on varying these parameters will be able to test these proposed scaling laws. Also, the weak dependence on velocity of the pre-factor for scaling in the direction parallel to the pulling direction needs to be explained.

Finally, it is worth placing the observed morphologies for the bubble raft in the context a number of other systems. First, the observed transition from DC to LT as the pulling speed is increased is similar

to the nanobridge simulation of liquid propane for which the transition occurs with higher background pressure [15]. The raises the important question of what sets the transition between the two modes. For the thermal systems, such as the nanobridge system, the transition is determined by fluctuations that are controlled by pressure. Therefore, one might expect that for the bubble raft, the transition is determined by fluctuations set by the pulling speed. This would be in direct analogy to the role of effective temperature in many driven, athermal systems [33–35]. In considering the source of the transition from DC to LT, it is interesting to note that the scaling appears to occur only below a minimum systems size, in this case when the width is less than approximately 25 bubbles. In shear flow studies of bubble rafts, one generally observes dynamics that can not be described by continuum mechanics if the size of the system is less than 15 to 20 bubbles [28, 36]. Since scaling regimes are generally understood in terms of instabilities in a continuum model of the system, understanding the scaling behavior in this small-scale system will be an important part of any future studies. Finally, bubble rafts are often used as models for amorphous systems. The change of average cone angle and pinch-off strain as a function of pulling velocity is consistent with simulations for necking instability of amorphous solids based on shear-transformation zones [37]. This result combined with the previously discussed cross-over from quasi-static to viscous flow strongly suggests that this system will be useful for future studies of pinch-off dynamics in a broad class of amorphous complex fluids and solids.

ACKNOWLEDGMENTS

We acknowledge the support of NSF-DMR-0907212 and Research Corporation. We thank Peter Taborek for the suggestion of fitting profiles to hyperbola and P. Taborek and Justin Burton for discussion of pinch-off in two-dimensions.

[1] J. Eggers, Physical Review Letters, **71**, 3458 (1993).
[2] D. T. Papageorgiou, Physics of Fluids, **7**, 1529 (1995).
[3] R. F. Day, E. J. Hinch, and J. R. Lister, Physical Review Letters, **80**, 704 (1998).
[4] I. Cohen, M. P. Brenner, J. Eggers, and S. R. Nagel, Physical Review Letters, **83**, 1147 (1999).
[5] A. Rothert, R. Richter, and I. Rehberg, Physical Review Letters, **87**, 084501 (2001).
[6] A. Rothert, R. Richter, and I. Rehberg, New Journal of Physics, **5**, 59 (2003).
[7] J. C. Burton, J. E. Rutledge, and P. Taborek, Physical Review Letters, **92**, 244505 (2004).
[8] Science, **302**, 1185 (2003), ISSN 1095-9203.
[9] J. Eggers, Reviews Of Modern Physics, **69**, 865 (1997), ISSN 0034-6861.
[10] J. Eggers and E. Villermaux, Reports on Progress in Physics, **71**, 036601 (2008), ISSN 0034-4885.
[11] J. C. Burton and P. Taborek, Physical Review Letters, **98**, 224502 (2007).
[12] J. C. Burton and P. Taborek, Physics of Fluids, **19**, 102109+ (2007).
[13] P. Constantin, T. F. Dupont, R. E. Goldstein, L. P. Kadanoff, M. J. Shelley, and S. M. Zhou, Physical Review E, **47**, 4169 (1993).
[14] M. Moseler and U. Landman, Science, **289**, 1165 (2000), ISSN 1095-9203.
[15] W. Kang and U. Landman, Phys. Rev. Lett., **98** (2007).
[16] J. R. Royer, D. J. Evans, L. Oyarte, Q. Guo, E. Kapit, M. E. Mobius, S. R. Waitukaitis, and H. M. Jaeger, Nature, **459**, 1110 (2009), ISSN 0028-0836.
[17] M. Z. Miskin and H. M. Jaeger, Proceedings of the National Academy of Sciences, **109**, 4389 (2012), ISSN 1091-6490.
[18] C. Bonnoit, T. Bertrand, E. Clément, and A. Lindner, Physics of Fluids, **24**, 043304 (2012).
[19] M. Hameed and J. F. Morris, SIAM Journal on Applied Mathematics.
[20] P. Coussot and F. Gaulard, Phys. Rev. E, **72**, 031409 (2005).
[21] F. M. Huisman, S. R. Friedman, and P. Taborek, Soft Matter, **8**, 6767 (2012).
[22] M. Arciniaga, C.-C. Kuo, and M. Dennin, Colloids and Surfaces A: Physicochemical and Engineering Aspects, **382**, 36 (2011), ISSN 09277757.
[23] C.-C. Kuo and M. Dennin, Journal of Rheology, **56**, 527+ (2012), ISSN 01486055.
[24] "See supplementary material for videos of particles dynamics and for raw data on the fitting exponents.".
[25] E. Pratt and M. Dennin, Physical Review E, **67**, 051402 (2003).
[26] U. J. Quaade and L. Oddershede, Europhysics Letters, **57**, 611 (2002).
[27] D. J. Durian, Physical Review Letters, **75**, 4780 (1995).
[28] M. Dennin, Physical Review E, **70**, 041406 (2004).
[29] M. Dennin, Colloids and Surfaces A: Physiochem and Eng. Asp., **263**, 76 (2005).
[30] Y. Wang, K. Krishan, and M. Dennin, Phys. Rev. E, **74**, 041405 (2006).
[31] M. Lundberg, K. Krishan, N. Xu, C. S. O'Hern, and M. Dennin, Phys. Rev. E, **77**, 041505 (2008).
[32] M. Lundberg, K. Krishan, N. Xu, C. S. O'Hern, and M. Dennin, Phys. Rev. E, **79**, 041405 (2009).
[33] I. K. Ono, C. S. O'Hern, D. J. Durian, S. A. Langer,

A. J. Liu, and S. R. Nagel, Physical Review Letters, **89**, 095703 (2002).
[34] C. S. O'Hern, A. J. Liu, and S. R. Nagel, Phys. Rev. Lett., **93**, 165702 (2004).
[35] N. Xu and C. S. O'Hern, Phys. Rev. Lett., **94**, 055701 (2005).
[36] J. Lauridsen, G. Chanan, and M. Dennin, Physical Review Letters, **93**, 018303 (2004).
[37] L. O. Eastgate, J. S. Langer, and L. Pechenik, Physical Review Letters, **90**, 045506 (2003).